ACS APPLIED MATERIALS & INTERFACES

Research Article

www.acsami.org

Sodium Chloride Template Synthesis of Cubic Tin Dioxide Hollow Particles for Lithium Ion Battery Applications

Rui Liu, Shengchun Yang,* Fei Wang,* Xuegang Lu, Zhimao Yang, and Bingjun Ding

School of Science, MOE Key Laboratory for Non-equilibrium Synthesis and Modulation of Condensed Matter, Shaan Xi, Xi'an Jiaotong University, 710049, People's Republic of China

Supporting Information

ABSTRACT: This paper describes a new synthesis and lithium ion charge−discharge property of tin dioxide (SnO_2) hollow nanocubes. SnO_2 is one of the best-known anode materials for lithium-ion battery application because of its high lithiation-delithiation capacity. Hollow nanostructures with high surface area are preferred, because they accommodate large volume changes and maintain the structural stability of electrode materials during charge−discharge cycles. The SnO_2 hollow cubes made in this study had a discharge capacity of up to 1783 mA h g^{-1} for the initial cycle and 546 mA h g^{-1} after 30 cycles at a current density of 0.2 C between 0.02 and 2.0 V (vs Li/Li^+).

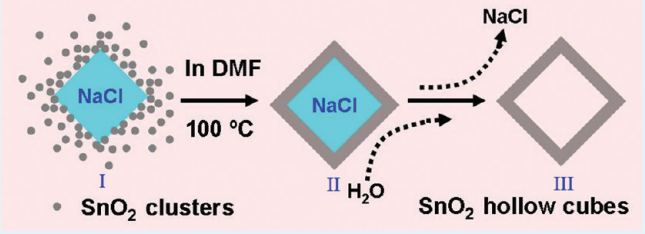

KEYWORDS: *tin dioxide, nanocubes, lithium ion battery, hollow structure*

1. INTRODUCTION

Tin dioxide (SnO_2), an n-type semiconductor with a band gap (E_g) of 3.6 eV,[1] has been widely studied in recent years because of its applications in photocatalysis,[2−4] gas sensor,[1,5,6] solar cell,[7−9] and battery.[10−16] For battery electrode, controlling the morphology of SnO_2 nanoparticles is important for improving conductivity, reducing lithium diffusion distance and accommodating the large volume changes.[15,17,18] Thus, it is advantagous to make SnO_2 hollow or porous in the preparation of electrodes.[19,20] Both 1D nanostructures and hollow structures have been explored for the design of new lithium ion battery electrodes using tin oxide-based materials. Much improved cycling ability and rate capability has been observed for these materials.[21−23] For example, short SnO_2 nanotube[23] shows a specific discharge capacity of 468 mA h g^{-1} after 30 cycles at a current density of 100 mA g^{-1}, and mesoporous SnO_2[21] has a surprising high capacity of 773 mA h g^{-1} after 50 cycles at a current density of 400 mA g^{-1}.

Strategies for preparing hollow nanostructures are largely based on templating approach.[5,10,24−27] Polystyrene and silica spheres are often used to make hollow structures through selective removal of these templates based on the difference in solubility between the template and shell materials.[5,12] Another method is based on the nanoscale Kirkendall effect,[28,29] which has been explored for making hollow nanoparticles (NPs) in relatively large quantity. In most cases, hollow structures have either spherical or tubular morphologies. For instance, SnO_2 nanoboxes were made by using Cu_2O templates.[15] However, in the above-mentioned strategies, the problems must be involved without exception:[12] (1) the prefabrication of template needs to control their morphologies carefully, leading to experiment much more complex; (2) The removal of the template through harsh approach, such as removing SiO_2 sphere via HF,[30] PMMA microspheres *via* organic solvent,[5] AAO template via NaOH,[31] brought the possibility of product deconstruction during the template removal process; (3) the multistep would cause the costly operations. In current research, we report a facile approach to the synthesis of uniform SnO_2 hollow cubes using in situ formed NaCl crystals as the templates. As NaCl is a water-soluble salt, removal of this material is much simpler than oxides due to large difference in water solubility between ionic compounds and oxides. On the other hand, the characteristic of cubic NaCl crystal offered a natural cube template without being finely controlled. The crystallinity of SnO_2 improved dramatically, while the hollow morphology remained intact after the treatment at high temperature. High reversible lithium ion discharge capacity and very good cycling performance were observed for anodes made of these SnO_2 hollow cubes.

2. EXPERIMENTAL SECTION

2.1. Synthesis of SnO_2 Hollow Cubes. In a typical synthesis, 0.5 g of poly(vinyl pyrrolidone) (PVP, Aldrich, MW = 40 000) and 1.5 g of $SnCl_4·5H_2O$ (Shanghai Shanpu Chemical Reagent, AR, 99%) were added to a three-neck round-bottom flask containing 60 mL of *N*,*N*-dimethylformamide (DMF, Shanghai Shanpu Chemical Reagent, AR, 99.5%). The experiment was performed under air atmosphere. The mixture was maintained at 100 °C for 1 h to remove the additional water in the solvent. Then, 0.29 g of sodium borohydride powder ($NaBH_4$, AR, 98.0%) was added with a stirring speed of 1000 rpm,

Received: December 12, 2011
Accepted: January 25, 2012
Published: January 25, 2012

while the solution color became black, indicating the Sn(IV) ions in DMF were reduced to Sn(0) through the following equation

$$SnCl_4 + NaBH_4 \rightarrow Sn + H_2 + NaCl + BCl_3 \quad (1)$$

After stirring for 20 min, the solution changed from black to gray and then to milklike color, indicating the formation of SnO_2 through eq 2.

$$Sn + O_2 \rightarrow SnO_2 \quad (2)$$

Temperature of the solution was then raised to 120 °C and kept for 1 h. After the reaction, the resulting white suspension was washed with distilled water and ethanol. The precipitate was separated from the mixture by centrifugation at 5000 rpm for 2 min. The supernatant was decanted and the white product was dispersed in 2 mL of distilled water, followed by centrifugation again at 5000 rpm for 2 min. The precipitate was collected and washed with another 2 mL of ethanol. This process was repeated three times. The final product was dried at 70 °C for 12 h.

2.2. Characterizations of Material Structures. Field-emission scanning electron microscopy (FE-SEM) images were taken on a JEOL JSM-7000F microscope. Energy dispersive X-ray (EDX) analysis was obtained with an Oxford INCA detector installed on the SEM. Transmission electron microscopy (TEM), high-resolution TEM (HR-TEM) micrographs, and selected-area electron diffraction (SAED) were taken on a JEOL JEM-3010 microscope at an accelerating voltage of 300 kV. The powder X-ray diffraction (PXRD) patterns were recorded using a BRUKER D8 ADVANCE X-ray diffractometer with a Cu Kα X-ray source (λ = 1.5405 Å). The oxidation states of the products were studied using X-ray photoelectron spectroscopy (XPS). The XPS spectra were obtained using Axis Ultra Kratos (UK) with monochromatic Al Kα radiation (150 W, 5 KV at 1486.6 eV). The chamber pressure for the spectrometer was kept at 1×10^{-9} Torr. Surface charge was corrected by referencing the spectra to C 1s peak for C−C bond at a binding energy at 284.5 eV.[38]

2.3. Characterizations of Electrochemical Properties. Electrochemical property was investigated using two-electrode test cells (Swagelok), which were assembled in an argon-filled glovebox. The working electrode was prepared by mixing the active materials, carbon black, and binder (polyvinylidene fluoride, PVDF) at a mass ratio of 80:10:10 in N-methyl pyrrolidinone (NMP). This slurry was deposited uniformly onto a piece of copper foil with a diameter of 10 mm and dried in vacuum at 100 °C for 12 h. Lithium foil was used as the counter electrode. The electrolyte was made of 1 M $LiPF_6$ in a mixture of ethylene carbonate (EC) and diethylene carbonate (DEC) at a volume ratio of 1:1. The galvanostatic charge and discharge tests were carried out at 25 °C using an Arbin BT2000 battery testing system. All the tests were cycled between 0.02 and 2.0 V (vs Li/Li^+) at a current density of 0.2 C (156 mA g^{-1}). The cyclic voltammograms (CV) were run at a scan rate of 0.2 mV s^{-1} between 0 and 2.0 V (vs Li/Li^+) on an Ametek VMC-4 electrochemical testing system.

3. RESULTS AND DISCUSSION

Figure 1 shows TEM micrographs and EDX analysis of the hollow cubes. The TEM data shows that average edge length of the cubes made was between 300 and 500 nm (Figure 1a). Holes were observed in the individual nanocube, further indicating the existence of hollow structures (Figure 1a, inset). TEM micrograph also shows the shell thickness was about 30 nm (Figure 1b and Figure S1a in the Supporting Information). SAED pattern of these hollow nanocubes contained diffraction rings, which were indexed to (101), (110), and (102) planes of rutile-type SnO_2 (Figure 1b, inset). The ring-like diffraction pattern suggests that shell was made of polycrystalline materials. The further enlarged TEM image showed that the shell of the hollow cubes was of a porous structure. HR-TEM micrograph reveals that the crystalline domain in the shell was between 1.5 and 3 nm, and the primary particles had short-range structural orders (Figure 1c). Two kinds of lattices were

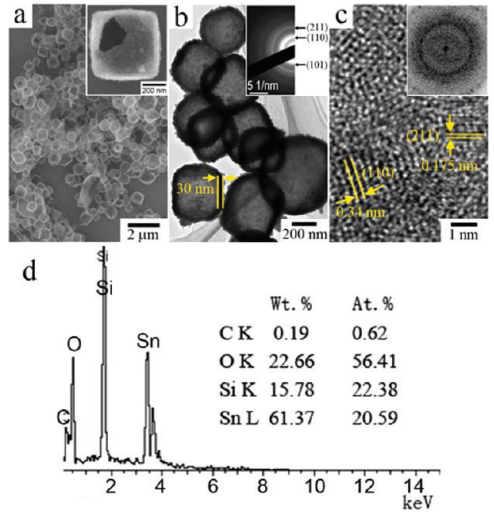

Figure 1. (a) FE-SEM image, (b, c) TEM micrographs, and (d) EDX of SnO_2 hollow cubes. The insets show (a) a single cube with a hole, (b) SAED, and (c) FFT analysis of the hollow cubes. The observed Si signal in the EDX pattern was from the substrate.

identified: one with *d*-spacing of 0.34 nm, which could be assigned to (110) plane of rutile-type SnO_2, and the other of 0.175 nm to (211) plane. The discrete spots in the fast Fourier transform (FFT) pattern indicate these domains were oriented randomly (Figure 1c, inset). Tin and oxygen were both clearly visible in the EDX analysis (Figure 1d).

Figure 2 shows the XPS survey scan and those for the Sn and O regions. The result indicates that the nanocubes contained

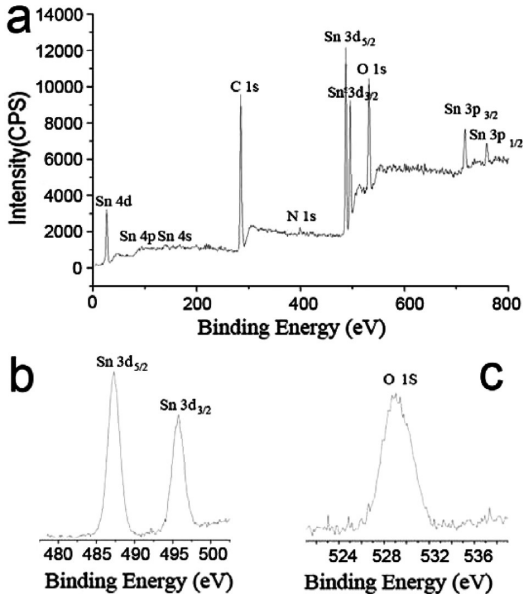

Figure 2. XPS spectra of (a) full scan, (b) Sn 3d, and (c) O 1s regions of as-made SnO_2 hollow cubes.

Sn, O, N, and C. The XPS spectrum in the range between 480 and 500 eV had two peaks: Sn $3d_{5/2}$ peak centered at 487.3 eV and Sn $3d_{3/2}$ peak at 495.7 eV. These two peaks are due to spin−orbital coupling of Sn 3d with an energy separation of 8.4 eV and a spin−orbital branching ratio of 1.67, which agreed well with those reported for SnO_2.[32,33] The binding energy for Sn $3d_{5/2}$ centered around 487.3 eV, indicating the tin was in the

Sn(IV) state (Figure 2b).[32] The single symmetric peak at 529.5 eV belonged to O 1s in SnO_2 (Figure 2c).

Figure 3a shows the PXRD patterns of the hollow cubes before and after the heat treatment at 500 °C in air. The as-made

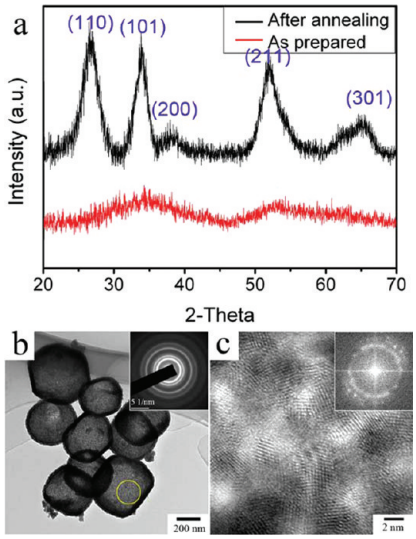

Figure 3. (a) XRD pattern, (b) TEM, and (c) HRTEM micrographs of SnO_2 hollow cubes after annealing at 500 °C for 3 h. The insets show (b) SAED and (c) FFT patterns.

sample shows broad diffraction bands, suggesting crystallinity of the material was low and the size of crystal domain was small. After the treatment, the diffraction peaks of SnO_2 became obvious, indicating the increased crystallinity and particle size. All the diffraction peaks could be assigned to the rutile-type of SnO_2. TEM micrograph shows that morphology of hollow cubes remained intact after the treatment (Figure 3b). The SAED patterns indicate that the crystal phase was rutile-type (inset in Figure 3b). High-resolution TEM micrograph shows that grain size was between 2 and 4 nm in diameter and the shell wall appeared to be porous (Figure 3c).

To understand the formation of hollow structures, we used those samples that were freshly recovered from the reaction solution. Samples were only briefly washed once with ethanol in order to minimize the removal of templates. Figure 4 shows

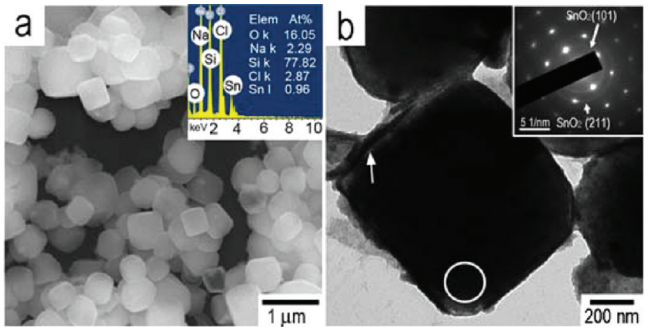

Figure 4. (a) SEM image and (b) TEM micrograph of the SnO_2 cubes with templates. The inset in a shows the corresponding EDX pattern, and the inset in b shows the SAED pattern taken from the circled region.

representative SEM image and TEM micrograph of the cubes after such gentle wash. As indicated in Figure 4a, the particles show a uniform contrast, indicating the templates remained inside the cubes (Figure 4a). Figure 4b show the representative TEM micrograph of the sample with the templates, from which an interface between the core and shell can be well identified (as shown by the arrow in Figure 4b), indicating a slight dissolution of NaCl occurred. EDX analysis reveals the existence of Sn, O, Na and Cl in these cubes, and the atomic ratio between Na and Cl was close to 1:1. The Si signal was from the substrate used in the measurement, and the excessive O signal could be attributed to the adsorbed PVP and oxygen molecules. The SAED pattern was composed of a set of well-defined diffraction spots and a series of diffraction rings (inset in Figure 4b). The spotted diffractions matched well with those of cubic phase of NaCl, while the light rings could be indexed to the (101) and (211) planes of rutile-type structure. The presence of NaCl crystals can be further proved through analysis of XRD pattern. Figure S2 in the Supporting Information showed the XRD pattern obtained from the sample only after gently washed with ethanol, in which the strong diffraction peaks can be well indexed to (111), (200), (220), (311), (222), (400), (420) and (422) planes of NaCl face-centered cubic (fcc) structure. The NaCl crystal could be dissolved readily in water, but was insoluble in ethanol. Thus, the formation process of cubic SnO_2 hollow particles can be illustrated as shown in Figure 5. At the stage I, the SnO_2 small

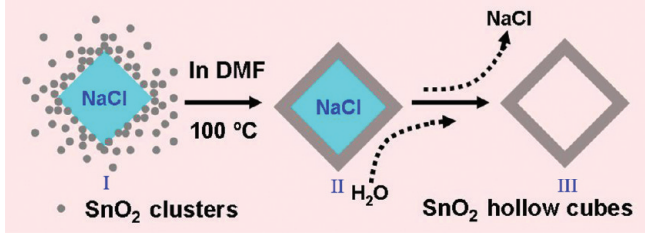

Figure 5. Schematic drawing of the formation of hollow cubic SnO_2 dioxide.

crystallites were deposited on the surface the in situ formed NaCl crystal, which would act as the template for the formation of cubes. At the second stage, the deposited SnO_2 small crystallites would begin to attach to each other because of the Oswald ripening occurring in organic solvent at 100 °C, which leads to the formation of shell layer on the surface of NaCl crystals. As the primary SnO_2 particles were very small, ion diffusion and mass transfer appeared not to be an issue for the formation of complete shells. Finally, the core of NaCl crystals was facilely removed by washing the products with water (stage III).

The concentration of PVP, which used as capping agent, was found to play an important role in formation of cubic SnO_2 hollow particles. As shown in Figure 6a, when PVP was absent in solvent, only SnO_2 nanoparticle aggregates can be obtained in final products. The increase of PVP amount showed a tendency to smooth the particle surface rather than affecting their sizes. As shown in Figure 6b, the lower concentration of PVP leads to a rough surface on the formed hollow particles. With the increase in PVP concentrations from 8.3 to 25 mg/mL, as shown in Figure 6c, d, their surface gradually becomes smooth and the average particle size still keep around 400 nm. However, when excess PVP was used during the preparation, the products showed a wide size distribution (Figure 6d), in which the polyhedrons with hollow interiors and large sizes (~ 1 μm) could be observed. These experimental phenomena can be probably attributed to the properties PVP molecules. It is well-known that PVP is a kind of commonly used capping agent

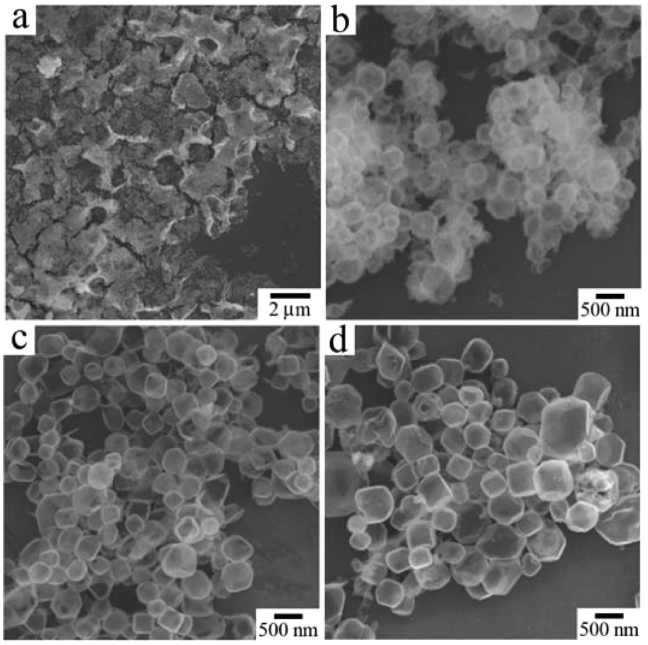

Figure 6. SEM images of SnO_2 samples synthesized with different PVP concentrations: (a) 0, (b) 4.2, (c) 8.3, and (d) 25 mg/mL.

in nanoparticle synthesis, in which the PVP molecules could absorbed on the surface of nanoparticles to restrain their further growth. In the current case, the growth of initial formed SnO_2 can be suppressed by PVP molecules, therefore, the SnO_2 nanoparticles with smaller sizes were more apt to deposit on the surface of NaCl crystals to form a compact shell layer. And on the other hand, decreasing sizes of SnO_2 nanoparticles could improve the Oswald ripening occurring. Thus the SnO_2 shells become smooth with the increase of PVP amount. However, the excessive amount of PVP might affect the crystallization of NaCl, which probably resulted in the formation of polyhedral NaCl crystals, and then lead to the formation of SnO_2 hollow polyhedrons.

The specific surface area and density functional theory (DFT) pore size distribution of SnO_2 hollow nanocubes were obtained based on the nitrogen isotherms carried out at 77 K (Figure 7). The results show that the as-made hollow nanocubes had a surface area of 230 m^2/g and an average pore size of around 3 nm, indicating that the shell of hollow cubes were of a porous structure, which also can be observed from their enlarged TEM image showing in Figure S1b in the Supporting Information. The hollow nanocubes had a BET surface area of 138 m^2/g after their annealing at 500 °C for 3 h (Figure 7b). And the average pore size showed a obvious increase, ranging from 2 nm to around 10 nm. This change can be ascribed to the growth of crystal in the shell as confirmed by PXRD. The growth of domains eliminated some porous structures, resulting in the decrease of specific surface area.

The electrochemical properties of SnO_2 hollow cubes were evaluated by cyclic voltammetry (CV). Figure 8a,b shows the

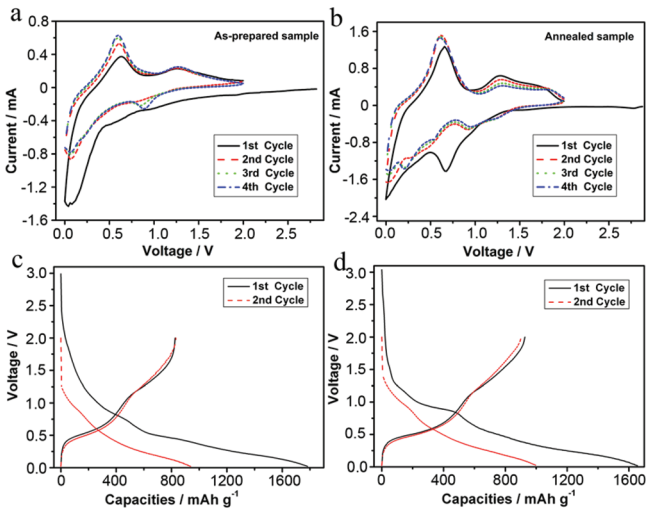

Figure 8. (a, b) CV and (c, d) voltage−capacity curves of the initial four cycles for (a, c) as-prepared and (b, d) annealed SnO_2 hollow cubes.

initial four CV cycles using the electrodes made from these two types of SnO_2 hollow cubes. In the very first cathodic scan, the peak at 0.7 V was due to the reduction of SnO_2 through the reaction with Li metal ($SnO_2 + 4Li^+ + 4e^- \leftrightarrow Sn + 2Li_2O$).[34] The broad band extending to 0 V corresponded to the formation of nonstoichiometric Li_xSn alloys ($Sn + xLi^+ + xe^- \leftrightarrow Li_xSn$, $0 \leq x \leq 4.4$).[17,18,34] This band split into distinguishable peaks after three cycles for the annealed samples (Figure 8b), whereas well-defined peaks at low cathodic voltage appeared, indicating the low overpotential and fast reaction kinetic for the annealed SnO_2 hollow cubes.[35]

Galvanostatic charge and discharge were tested at a rate of 0.2 C between 0.02 and 2.0 V (vs Li/Li^+). The as-made SnO_2 hollow cubes had an initial charge capacity of 826 mAh g^{-1} and discharge capacity of 1783 mA h g^{-1} (Figure 8c). The low initial Coulomb efficiency (46%) was attributed mainly to the formation of Li_2O, solid electrolyte interface (SEI layer), and electrolyte decomposition.[17,18,36] For the SnO_2 hollow cubes

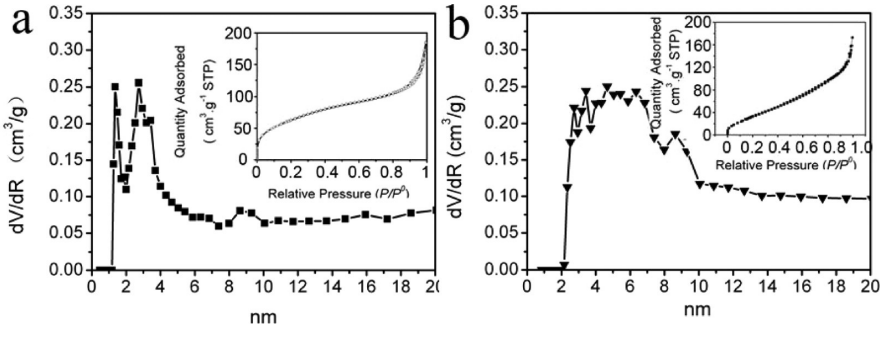

Figure 7. DFT pore-size distribution analysis based on the desorption curves of nitrogen isotherms (inset) for (a) as-made and (b) annealed SnO_2 hollow cubes.

dx.doi.org/10.1021/am201756m | ACS Appl. Mater. Interfaces 2012, 4, 1537−1542

after annealing at 500 °C, the charge capacity increased to 927 mA h g^{-1}, whereas the discharge capacity decreased to 1654 mA h g^{-1} (Figure 8d). The observed reduction in the initial irreversible reaction and the improvement in Coulomb efficiency were mostly due to the growth in crystal size and the reduction of specific surface area after annealing.[36]

Figure 9 shows the discharge capacity of SnO_2 hollow cubes before and after the annealing. After the initial cycle, the discharge

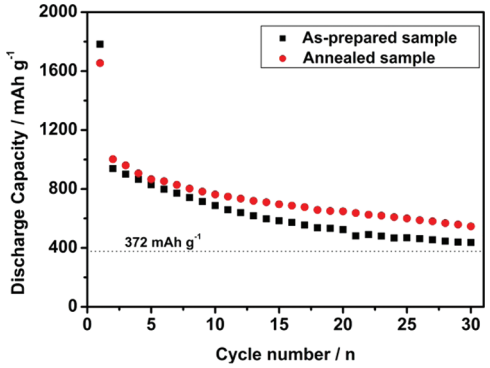

Figure 9. Discharge capacity as a function of cycle number of as-prepared (black square) and annealed (red circle) SnO_2 hollow cubes.

capacity for annealed hollow cubes remained high and reached 1002 mAh g^{-1} for its second cycle. Such high lithium storage capacity could be due to the high specific surface areas of the hollow cubes, a phenomenon being observed in SnO_2 nanoboxes[15] and nanosheets.[16] The discharge capacity leveled off to 546 mA h g^{-1} after 30 cycles. This capacity is better than unannealed SnO_2 electrodes and higher than the theoretical value of commercial graphite (372 mA h g^{-1}).[37] The improved cycling performance of annealed SnO_2 hollow cubes should be ascribed to the hollow structures which is beneficial for accommodating the severe volume changes during the lithiation/delithiation processes. For the as-synthesized hollow cubes, the capacity decreased fast than the annealed, though the capacity after 30 cycles was still higher than that of graphite. The difference between the as-made and annealed samples was likely related to the crystalline and degree of hydration of tin oxide in the hollow cubes.[15]

4. SUMMARY

In summary, we present a new approach to the preparation of uniform SnO_2 hollow cubes that have large lithium storage capacity at relatively high charge–discharge rates. Using common salt crystal template is a facile and scalable synthesis of well-defined metal oxides with high surface area to volume ratio. This work opens up new horizons for the development of novel classes of SnO_2 nanostructures for lithium-ion battery applications.

■ ASSOCIATED CONTENT

Supporting Information

TEM and XRD analyses of the SnO_2 hollow structures. This material is available free of charge via the Internet at http://pubs.acs.org.

■ AUTHOR INFORMATION

Corresponding Author

*Fax: 86-29-82665995. Tel: 86-29-82663034. E-mail: ysch1209@mail.xjtu.edu.cn (S.Y.); feiwang@mail.xjtu,.edu.cn (F.W.).

Notes

The authors declare no competing financial interest.

■ ACKNOWLEDGMENTS

This work was supported by the National Natural Science Foundation of China (50901056, No.51002117 and No.51172178), Doctoral Fund for New Teachers (20090201120053), and the Fundamental Research Funds for the Central Universities.

■ REFERENCES

(1) Miao, Z. J.; Wu, Y. Y.; Zhang, X. R.; Liu, Z. M.; Han, B. X.; Ding, K. L.; An, G. M. *J. Mater. Chem.* **2007**, *17*, 1791–1796.
(2) Coelho, M. G.; de Lima, G. M.; Augusti, R.; Maria, D. A.; Ardisson, J. D. *Appl. Catal., B* **2010**, *96*, 67–71.
(3) Kansal, S. K.; Singh, M.; Sud, D. *J. Hazard. Mater.* **2007**, *141*, 581–590.
(4) Zhang, H. J.; Chen, G. H.; Bahnemann, D. W. *J. Mater. Chem.* **2009**, *19*, 5089–5121.
(5) Chang, Y. E.; Youn, D. Y.; Ankonina, G.; Yang, D. J.; Kim, H. G.; Rothschild, A.; Kim, I. D. *Chem. Commun.* **2009**, 4019–4021.
(6) Kim, H. R.; Choi, K. I.; Kim, K. M.; Kim, I. D.; Cao, G. Z.; Lee, J. H. *Chem. Commun.* **2010**, *46*, 5061–5063.
(7) Liu, J. Y.; Luo, T.; Mouli, T. S.; Meng, F. L.; Sun, B.; Li, M. Q.; Liu, J. H. *Chem. Commun.* **2010**, *46*, 472–474.
(8) Qian, J. F.; Liu, P.; Xiao, Y.; Jiang, Y.; Cao, Y. L.; Ai, X. P.; Yang, H. X. *Adv. Mater.* **2009**, *21*, 3663–3667.
(9) Snaith, H. J.; Ducati, C. *Nano Lett.* **2010**, *10*, 1259–1265.
(10) Lou, X. W.; Li, C. M.; Archer, L. A. *Adv. Mater.* **2009**, *21*, 2536–2539.
(11) Han, S. J.; Jang, B. C.; Kim, T.; Oh, S. M.; Hyeon, T. *Adv. Funct. Mater.* **2005**, *15*, 1845–1850.
(12) Deng, D.; Lee, J. Y. *Chem. Mater.* **2008**, *20*, 1841–1846.
(13) Lou, X. W.; Wang, Y.; Yuan, C. L.; Lee, J. Y.; Archer, L. A. *Adv. Mater.* **2006**, *20*, 2325–2329.
(14) Lee, K. T.; Lytle, J. C.; Ergang, N. S.; Oh, S. M.; Stein, A. *Adv. Funct. Mater.* **2005**, *15*, 547–556.
(15) Wang, Z. Y.; Luan, D. Y.; Boey, F. Y. C.; Lou, X. W. *J. Am. Chem. Soc.* **2011**, *133*, 4738–4741.
(16) Wang, C.; Zhou, Y.; Ge, M. Y.; Xu, X. B.; Zhang, Z. L.; Jiang, J. Z. *J. Am. Chem. Soc.* **2010**, *132*, 46–47.
(17) Wang, C. M.; Xu, W.; Liu, J.; Zhang, J. G.; Saraf, L. V.; Arey, B. W.; Choi, D.; Yang, Z. G.; Xiao, J.; Thevuthasan, S.; Baer, D. R. *Nano Lett.* **2011**, *11*, 1874–1880.
(18) Huang, J. Y.; Zhong, L.; Wang, C. M.; Sullivan, J. P.; Xu, W.; Zhang, L. Q.; Mao, S. X.; Hudak, N. S.; Liu, X. H.; Subramanian, A.; Fan, H. Y.; Qi, L.; Kushima, A.; Li, J. *Science* **2010**, *330*, 1515–1520.
(19) Wang, Y.; Cao, G. Z. *Adv. Mater.* **2008**, *20*, 2251–2269.
(20) Kim, M. G.; Cho, J. *Adv. Funct. Mater.* **2009**, *19*, 1497–1514.
(21) Kim, H.; Cho, J. *J. Mater. Chem.* **2008**, *18*, 771–775.
(22) Park, M. S.; Wang, G. X.; Kang, Y. M.; Waxler, D.; Dou, S. X.; Liu, H. K. *Angew. Chem., Int. Ed.* **2007**, *46*, 750–753.
(23) Ye, J. F.; Zhang, H. J.; Yang, R.; Li, X. G.; Qi, L. M. *Small* **2010**, *6*, 296–306.
(24) Caruso, F.; Caruso, R. A.; Mohwald, H. *Science* **1998**, *282*, 1111–1114.
(25) Lee, W. J.; Park, M. H.; Wang, Y.; Lee, J. Y.; Cho, J. *Chem. Commun.* **2010**, *46*, 622–624.
(26) Liang, H. W.; Liu, S.; Gong, J. Y.; Wang, S. B.; Wang, L.; Yu, S. H. *Adv. Mater.* **2009**, *21*, 1850–1854.
(27) Sun, Y. G.; Mayers, B.; Xia, Y. N. *Adv. Mater.* **2003**, *15*, 641–646.
(28) Yin, Y. D.; Rioux, R. M.; Erdonmez, C. K.; Hughes, S.; Somorjai, G. A.; Alivisatos, A. P. *Science* **2004**, *304*, 711–714.
(29) Hung, L. I.; Tsung, C. K.; Huang, W. Y.; Yang, P. D. *Adv. Mater.* **2010**, *22*, 1910–1914.
(30) Lou, X. W.; Yuan, C.; Archer, L. A. *Small* **2007**, *3*, 261–265.
(31) Wang, Y.; Zeng, H. C.; Lee, J. Y. *Adv. Mater.* **2006**, *18*, 645–649.
(32) Batzill, M.; Diebold, U. *Prog. Surf. Sci.* **2005**, *79*, 47–154.

(33) Moulder, J.; Stickie, W.; Sobal, P.; Bomber, K. *Handbook of X-ray Photoelectron Spectroscopy*; Perkin Elmer: Eden Prairie, MN, 1992.
(34) Courtney, I. A.; Dahn, J. R. *J. Electrochem. Soc.* **1997**, *144*, 2045−2052.
(35) Winter, M.; Besenhard, J. O.; Spahr, M. E.; Novak, P. *Adv. Mater.* **1998**, *10*, 725−763.
(36) Winter, M.; Besenhard, J. O. *Electrochim. Acta* **1999**, *45*, 31−50.
(37) Idota, Y.; Kubota, T.; Matsufuji, A.; Maekawa, Y.; Miyasaka, T. *Science* **1997**, *276*, 1395−1397.
(38) Deng, Z. T.; Peng, B.; Chen, D.; Tang, F. Q.; Muscat, A. J. *Langmuir* **2008**, *24*, 11089−11095.